On

Supporting information for

Unique multiphthalocyanine coordination systems: vibrationally hot excited states and charge transfer states that power high energy triplet charge separated states

Jan Joseph,[a] Leandro M. O. Lourenço,*[b] João P. C. Tomé,*[c] Tomás Torres,*[def] Dirk M. Guldi*[a]

[a]*Department of Chemistry and Pharmacy and Interdisciplinary Center for Molecular Materials, Friedrich-Alexander-Universität, 91058 Erlangen, Germany.*
[b]*LAQV-REQUIMTE and Department of Chemistry, University of Aveiro, 3810-193 Aveiro, Portugal.*
[c]*CQE, Institute of Molecular Sciences, and Departamento de Engenharia Química, Instituto Superior Técnico, Universidade de Lisboa, 1049-001 Lisboa, Portugal.*
[d]*Departamento de Química Orgánica, Universidad Autónoma de Madrid, Cantoblanco, 28049 Madrid, Spain.*
[e]*Institute for Advanced Research in Chemical Sciences (IAdChem), Universidad Autonoma de Madrid (UAM), 28049 Madrid, Spain.*
[f]*IMDEA-Nanociencia, c/Faraday, 9, Cantoblanco, 28049 Madrid, Spain.*

Contents

1. Experimental section

General information

^{1}H NMR spectra were recorded with a *Bruker Avance-300* spectrometer at 300.13 MHz, using tetramethylsilane as internal reference. The chemical shifts were expressed in δ (ppm) and the coupling constants (*J*) in Hz. Steady-state absorption spectra were recorded with a Perkin-Elmer Lambda 35. Elemental analyses for C, H and N were performed with a Truspec Micro CHNS 630−200−200 equipment at the Department of Chemistry, University of Aveiro. Analysis Parameters: sample amount between 1 and 2 mg; combustion furnace temperature = 1075 °C for 4 min; after burner temperature = 850 °C. Detection methods: carbon, hydrogen, sulphur by Infrared absorption detection method, and nitrogen by thermal conductivity detection method. Gases required: carrier, helium; combustion, oxygen; pneumatic, compressed air. Steady-state emission spectra were recorded in a Fluoromax-3-spectrometer from HORIBA Jobin Yvon. All samples were measured in a fused quartz glass cuvette with 10 mm light path. Analytical TLC was carried out on precoated silica gel sheets (Merck, 60, 0.2 mm). Column chromatography was carried out over silica gel (Merck, 63–200 mesh). Molecular extrusion column chromatography was carried out over Bio-beads^{TM} S-X1 Beads (200-400 Mesh, 100 g), Bio-Rad Laboratories, Inc. MALDI-MS mass spectra were acquired using a MALDI-TOF/TOF Applied Biosystems 4800 Proteomics Analyzer (Applied Biosystems, Framingham, MA, USA) instrument equipped with a nitrogen laser emitting at 337 nm. Prior to MALDI-MS analysis, 4 μL of matrix, dithranol (10 mg.mL^{-1} in methanol/TFA 0.1%) were mixed with 2 μL of the dye solution in dichloromethane/methanol (≈10 μg.mL^{-1}), and 1 μL of this mixture was deposited on the MALDI plate and let to dry. MALDI-MS spectra were acquired in the positive ion reflector mode using delayed extraction in the mass range between 600 and 4500 Da with ca. 1500 laser shots. For the following acquisition of tandem mass spectra, a collision energy of 2 keV was used to induce fragmentation, and air was used as collision gas.

Steady-state spectroscopy

UV-Vis absorption measurements at room temperature were performed in a 10 × 10 mm cuvette with a Lambda 2 double beam instrument (Perkin-Elmer). Fluorescence measurements were performed in a 10 × 10 mm cuvette with a Fluoromax 3 spectrometer (HORIBA Yobin).

Time resolved spectroscopy

Time Correlated Single-Photon Counting (TCSPC) experiments were carried out on an Edinburgh FS5 spectrofluorometer. The samples were excited at 370-380 nm with a UV picosecond laser from Picoquant (PDL 800-B). Each measurement was performed using a 10 × 10 mm quartz cuvette.

Femtosecond transient absorption spectra were obtained with a Ti:sapphire laser system CPA-2101 (Clark-MXR), Inc.) in combination with a Helios TAPPS detection unit from Ultrafast Inc. The initial laser excitation wavelength is 775 nm with a pulse width of 150 fs. The used excitation wavelength was 387 nm on one hand, which was generated with a SHG crystal, and 694 nm on the other hand, which was generated using a non-collinear optical parametric amplifier (NOPA, Clark-MXR). For the generation of the white light a sapphire crystal of adequate thickness was used. The detection was carried out with two charge-coupled device (CCD) cameras, each for a specific measuring range. The spectral window is therefore 415 to 770 nm and 770 to 1600 nm. The delay line allows spectral acquisition up to time delays of 5500 ps. All samples were measured in a fused quartz glass cuvette with a thickness of 2 mm at room temperature. Data was acquired with the software HELIOS Visible/nIR (Newport / Ultrafast Systems).

Electrochemistry

Square-wave voltammetry studies were performed with an Autolab PGSTAT101 potentiostat at room temperature. Degassed DCM (bubbled with argon for 20 min) was used as solvent and 0.1 M tetra-*n*-butylammonium hexafluorophosphate (*n*-Bu_4NPF_6) as supporting electrolyte. A gold

electrode was used as the working electrode, a platinum wire as the counter electrode and an Ag-wire as quasi-reference electrode. All potentials were corrected against the Fc/Fc^+ redox couple.

Spectroelectrochemical measurements at room temperature were performed using a Metrohm PGSTAT101 potentiostat in combination with a Cary 5000 double beam spectrometer (Varian). A commercially available thin layer cell (OMNI-CELL SPECAC) with CaF_2 windows and platinum mesh as working electrode, silver wire as quasi-reference electrode and platinum counter electrode was employed. Degassed DCM (bubbled with argon for 20 min) was used as solvent and 0.1 M tetra-*n*-butylammonium hexafluorophosphate (*n*-Bu_4NPF_6) as supporting electrolyte.

Synthesis and Characterization

Synthesis of H_2PcSPy

In a 25 mL round-bottom flask, a solution containing 4-thiopyridylphthalonitrile (103.5 mg, 0.436 mmol), commercial 4-*tert*-butylphthalonitrile (552.9 mg, 3.000 mmol, 6.9 equiv.) and lithium (25.5 mg, 3.674 mmol, 8.4 equiv.) in 5 mL of 1-pentanol was heated at 120 ºC under N_2 atmosphere. After 48 h, the TLC control confirmed the reaction was complete. The reaction solution was then distilled until dryness, the crude product dissolved in CH_2Cl_2 and purified by silica chromatography column using a mixture of CH_2Cl_2/MeOH/ (95:5) as eluent. The desired product was obtained from precipitation in a mixture of $CHCl_3$/Hexane, filtered and washing with hexane. **H_2PcSPy** (150.5 mg, 0.190 mmol) was obtained in 45.1% yield. ^{1}H NMR (300.13 MHz, $CDCl_3$): δ -4.25 – -4.02 (m, 2H, NH), 1.85 (s, 27H, ^{t}Bu), 7.38 (d, J = 6.3 Hz, 2H, SPy-*o*-H), 8.00 – 8.06 (m, 4H, Pc β-H), 8.39 – 8.57 (m, 8H, Pc α-H), 8.63 – 8.68 (m, 2H, SPy-*m*-H). HRMS: *m/z* calculated for $C_{49}H_{45}N_9S$: 791.3519; found: 792.3564 $[M+H]^+$. Elemental analysis; Calcd for $C_{49}H_{45}N_9S{\cdot}2H_2O$: C, 69.56; H, 6.08; N, 14.90; O, 5.67; S, 3.79; found: C, 70.27; H, 5.59; N, 14.98; S, 3.81. UV-Vis (CH_2Cl_2), λ_{max} (log ε): 342 (4.54), 614 (4.23), 641(4.40), 670 (4.71), 690 (4.76) nm.

Synthesis of ZnPcSPy

In a 25 mL round-bottom flask, a solution containing **H_2PcSPy** (45.1 mg, 0.057 mmol) and zinc acetate (60.8 mg, 0.331 mmol, 5.8 equiv.) was stirred in 4 mL of methanol/dichloromethane (1:1) heated at 45 ºC under N_2 atmosphere. After 24 h, the TLC control confirmed the reaction was complete. The reaction solution was then distilled until dryness, the crude product dissolved in CH_2Cl_2 and purified by silica chromatography column using a mixture of CH_2Cl_2/MeOH (95:5) as eluent. The desired product was obtained from precipitation in a mixture of $CHCl_3$/Hexane, filtered and washing with hexane. **ZnPcSPy** (42.0 mg, 0.049 mmol) was obtained in 86.2% yield. ^{1}H NMR (300.13 MHz, $CDCl_3$: δ 1.34 (s, 27H, ^{t}Bu-H), 7.52 – 7.89 (m, 8H, Pc α-H), 7.90 (d, J = 1.1 Hz, 2H, SPy-*o*-H), 8.05 (d, J = 1.1 Hz, 2H, SPy-*m*-H), 8.17 – 8.48 (m, 4H, H_2Pc β-H). MS: *m/z* calculated for $C_{49}H_{43}N_9SZn$: 853.3; found: 854.6 $[M+H]^+$. UV-Vis (CH_2Cl_2), λ_{max} (log ε): 354 (4.64), 664 (4.74), 689 (4.83) nm.

Note: The synthesis of **H_2PcSPy$_4$**[1] and **ZnPcSPy$_4$**[2] were made accordingly with the literature.

Synthesis of the supramolecular dyad 1

H_2PcSPy (50.1 mg, 0.063 mmol) and **RuPc** (59.2 mg, 0.068 mmol, 1.1 equiv.) were stirred in CH_2Cl_2 (5 mL) along 48 h at 30 ºC. The reaction solution was then concentrated on a rotary evaporator and separated by gel permeation chromatography (Bio-Beads S-X1) using CH_2Cl_2 as eluent. The first obtained fraction was identified as being compound **1** (95.8 mg, 0.068 mmol) afforded in 91.6% yield, as a deep blue solid. ^{1}H NMR (300.13 MHz, $CDCl_3$): δ -3.36 – -3.28 (m, 2H, NH), 1.77 (s, 63H, ^{t}Bu-H), 4.93 – 4.89 (m, 2H, SPy-*o*-H), 7.90 – 8.03 (m, 16H, RuPc β-H, H_2Pc α-H and H_2Pc β-H), 8.62 – 8.68 (m, 2H, SPy-*m*-H), 8.85 – 9.26 (m, 8H, RuPc α-H). HRMS: *m/z* calculated for $C_{98}H_{93}N_{17}ORuS$: 1657.65132; found: 1658.6572 $[M+H]^+$. Elemental analysis; Calcd for $C_{98}H_{93}N_{17}ORuS$: C, 70.99; H, 5.65; N, 14.36; O, 0.96; Ru, 6.10; S, 1.93; found: C, 71.45; H, 5.81; N, 14.27; S, 0.92. UV-Vis (CH_2Cl_2), λ_{max} (log ε): 341 (4.89), 586 (4.73), 647 (5.39), 671 (5.09), 688 (4.70) nm.

---

[1] K. A. D. F. Castro, F. Figueira, F. A. Almeida Paz, J. P. C. Tomé, R. S. da Silva, S. Nakagaki, M. G. P. M. S. Neves, J. A. S. Cavaleiro and M. M. Q. Simões, *Dalt. Trans.*, **2019**, *48*, 8144–8152.

[2] J. B. Pereira, E. F. A. Carvalho, M. A. F. Faustino, R. Fernandes, M. G. P. M. S. Neves, J. A. S. Cavaleiro, N. C. M. Gomes, Â. Cunha, A. Almeida and J. P. C. Tomé, *Photochem. Photobiol.*, **2012**, *88*, 537–547.

Synthesis of the supramolecular dyad 2

The hybrid **1** (27.0 mg, 0.016 mmol) and zinc acetate (4.1 mg, 0.022 mmol, 1.4 equiv.) were stirred in a mixture of CH_2Cl_2/MeOH/ (9:1, 5 mL) for 48 h at reflux and under N_2 atmosphere. After that, the mixture was concentrated until dryness, dissolved in CH_2Cl_2 and separated by gel permeation chromatography (Bio-Beads S-X1) using CH_2Cl_2 as eluent. The desired zinc complex **2** (25.1 mg, 0.015 mmol) was isolated in 83.0% yield as a deep blue solid. ^{1}H NMR (300.13 MHz, $CDCl_3$): δ 1.76 (s, 63H, ^{t}Bu-H), 4.74 – 5.04 (m, 2H, SPy-*o*-H), 7.91 – 8.10 (m, 8H, ZnPc β-H and RuPc β-H), 8.85 – 9.56 (m, 18H, ZnPc α-H, RuPc α-H and SPy-*m*-H). HRMS: *m/z* calculated for $C_{98}H_{91}N_{17}ORuSZn$: 1719.56482; found: 1721.5705 $[M+2H]^+$. Elemental analysis; Calcd for $C_{98}H_{91}N_{17}ORuSZn.5H_2O$: C, 64.98; H, 5.62; N, 13.14; O, 5.30; Ru, 5.58; S, 1.77; Zn, 3.61; found: C, 65.45; H, 5.22; N, 12.40; S, 1.29. UV-Vis (CH_2Cl_2), λ_{max} (log ε): 346 (5.00), 586 (4.62), 648 (5.29), 687 (5.16) nm.

Note: Coordinative interactions between ZnPcSPy may occur in solution and is well-documented in the literature.[3] In terms of synthesis of ZnPcSPy-RuPc **2**, it was prepared from H_2PcSPy-RuPc **1** with the well-known high Ru-SPy coordination affinity and followed by zinc metalation to avoid Zn-SPy coordination effects. During the purification by means of Biobeads column chromatography with dichloromethane the main fraction corresponded to **2** with 83% yield. Most probably the interaction of Ru-SPy binding is very strong in solution relatively to a possible Zn-SPy binding because after product isolation a coherent elemental analysis data was obtained.

Synthesis of the supramolecular array 3

H_2PcSPy$_4$ (10.1 mg, 0.011 mmol) and **RuPc** (40.2 mg, 0.046 mmol, 4.2 equiv.) were stirred in CH_2Cl_2 (5 mL) along 48 h at 30 ºC. The reaction solution was then concentrated, on a rotary evaporator, and separated by gel permeation chromatography (Bio-Beads S-X1) using CH_2Cl_2 as eluent. The first obtained fraction was identified as being compound **3** (43.4 mg, 0.010 mmol) afforded in 92.5% yield, as a deep blue solid. ^{1}H NMR (300.13 MHz, $CDCl_3$): δ 1.66 – 1.76 (m, 144H, ^{t}Bu-H), 4.93 – 5.03 (m, 8H, SPy-*o*-H), 7.90 – 8.13 (m, 28H, RuPc α-H, H_2Pc α-H and H_2Pc

[3] F. Battistin, A. Vidal, P. Cavigli, G. Balducci, E. Iengo, E. Alessio, *Inorg. Chem.*, **2020**, *59*, 4068−4079.

β-H), 9.16 – 9.33 (m, 40H, RuPc β-H and SPy-*m*-H). . Elemental analysis; Calcd for $C_{248}H_{222}N_{44}O_4Ru_4S_4$: C, 67.46; H, 5.07; N, 13.96; O, 1.45; Ru, 9.16; S, 2.90; found: C, 67.42; H, 5.00; N, 12.90; S, 2.59. UV-Vis (CH_2Cl_2), λ_{max} (log ε): 345 (5.47), 586 (5.09), 647 (5.76), 702 (5.55) nm.

Synthesis of the supramolecular array 4

The hybrid **3** (20.8 mg, 0.005 mmol) and zinc acetate (10.4 mg, 0.057 mmol, 11.4 equiv.) were stirred in a mixture of CH_2Cl_2/MeOH (9:1, 5 mL) for 48 h at reflux and under N_2 atmosphere. After that, the mixture was concentrated until dryness, dissolved in CH_2Cl_2, and was purified by molecular extrusion using CH_2Cl_2 as eluent. The desired zinc complex **4** (19.0 mg, 0.004 mmol) was isolated in 90% yield as a deep blue solid. ^{1}H NMR (300.13 MHz, $CDCl_3$): δ 2.11 (s, 144H, ^{t}Bu-H), 5.01 – 5.13 (m, 8H, SPy-*o*-H), 7.73 – 8.23 (m, 28H, RuPc α-H, ZnPc α-H and ZnPc β-H), 8.89 – 9.55 (m, 40H, RuPc β-H and SPy-*m*-H). UV-Vis (CH_2Cl_2), λ_{max} (log ε): 345 (5.19), 586 (5.11), 648 (5.77), 681 (5.23) nm.

2. Structures of reference compounds

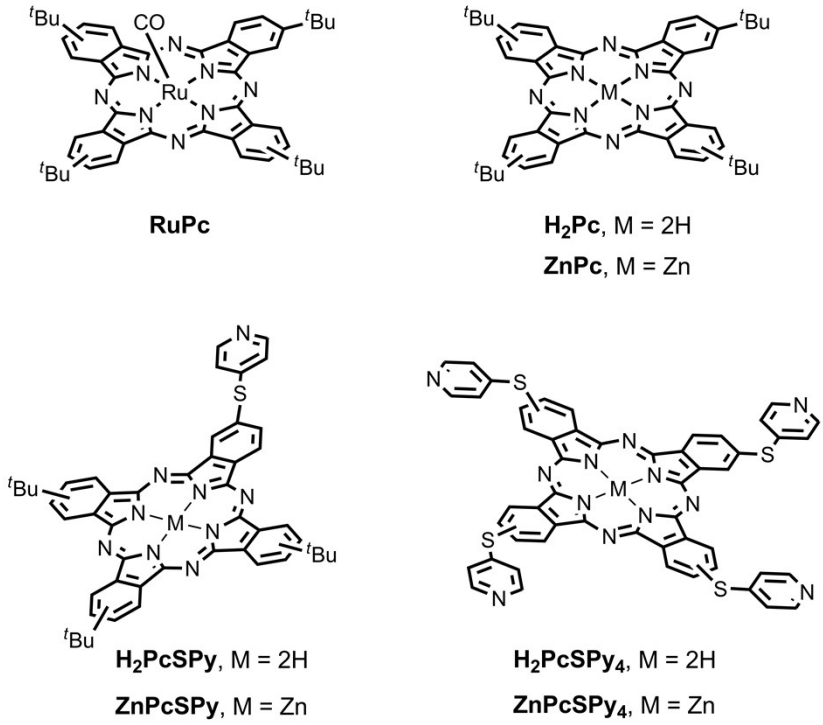

Fig. S1 Structures of **RuPc**, **H_2Pc**, **ZnPc**, **H_2PcSPy**, **ZnPcSPy**, **H_2PcSPy$_4$** and **ZnPcSPy$_4$**.

3. Structural characterization

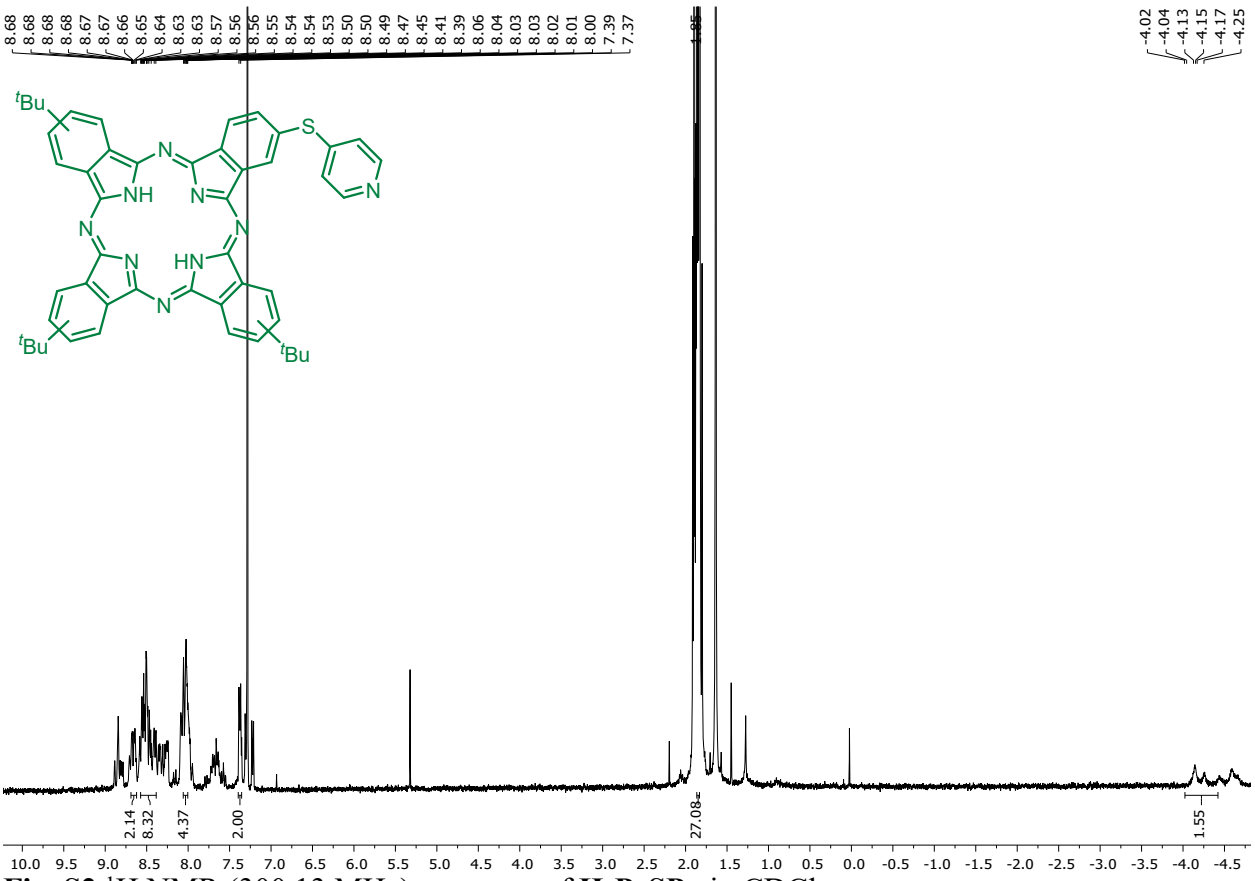

Fig. S2 ^{1}H NMR (300.13 MHz) spectrum of **H_2PcSPy** in $CDCl_3$.

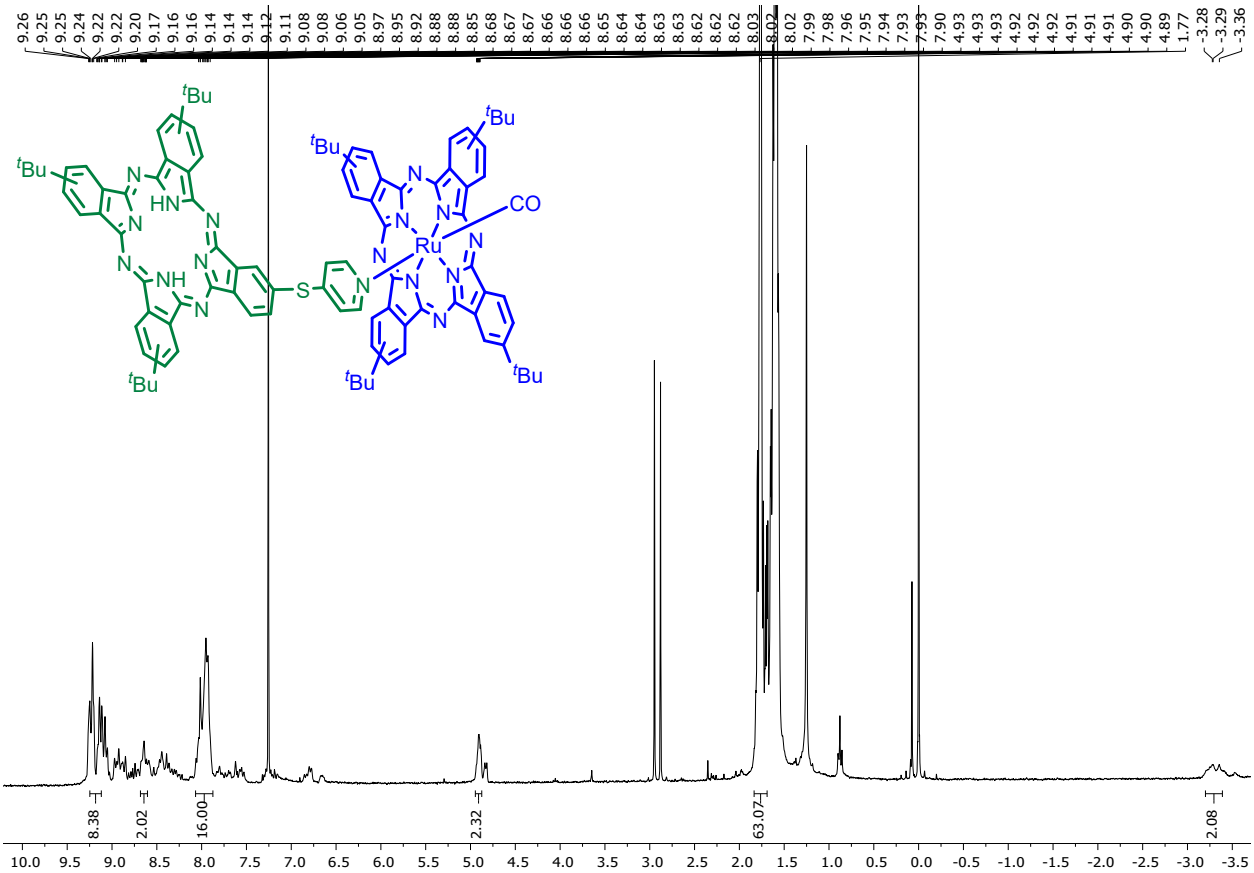

Fig. S3 ^{1}H NMR (300.13 MHz) spectrum of **1** in $CDCl_3$.

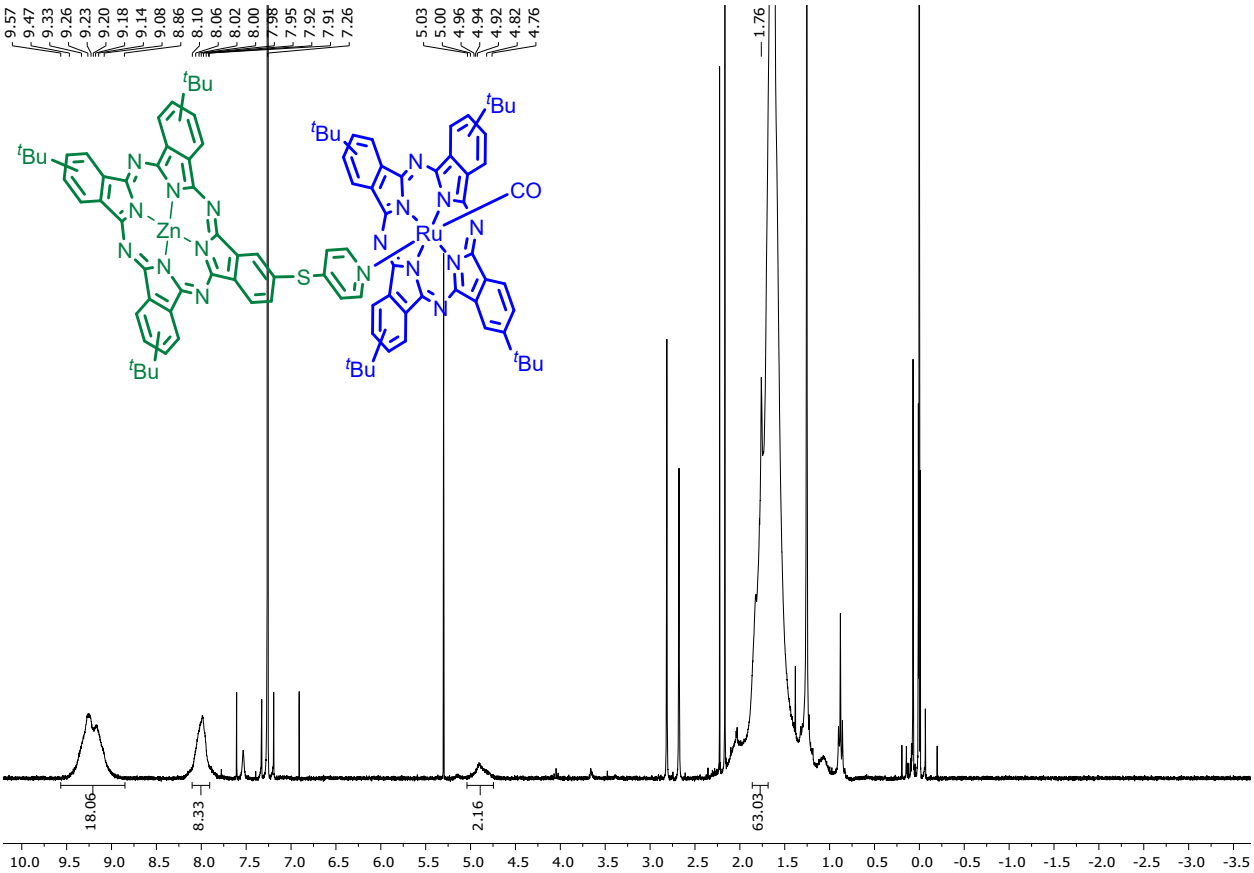

Fig. S4 ^{1}H NMR (300.13 MHz) spectrum of **2** in $CDCl_3$.

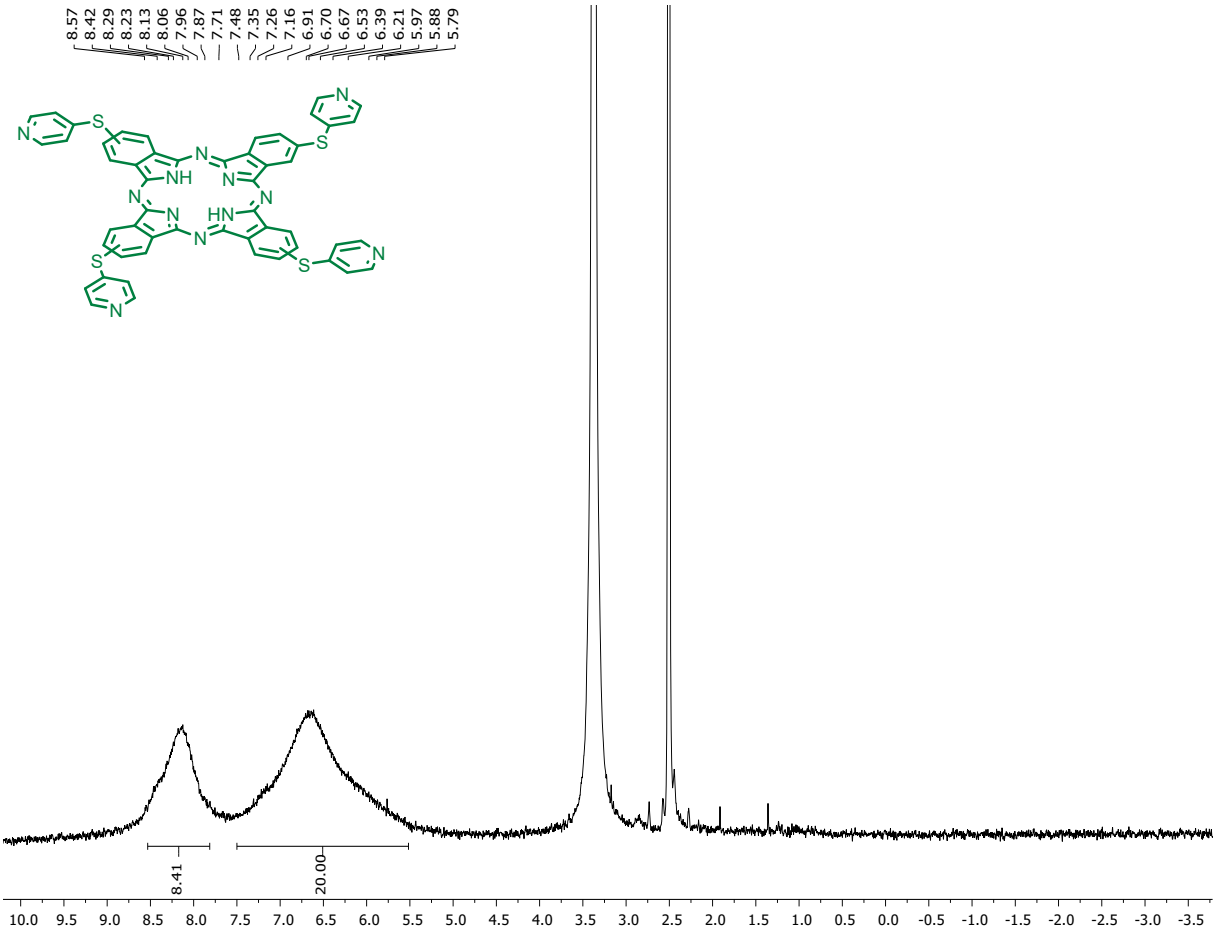

Fig. S5 ^{1}H NMR (300.13 MHz) spectrum of **$H_2PcH_{12}SPy_4$** in DMSO-d_6.

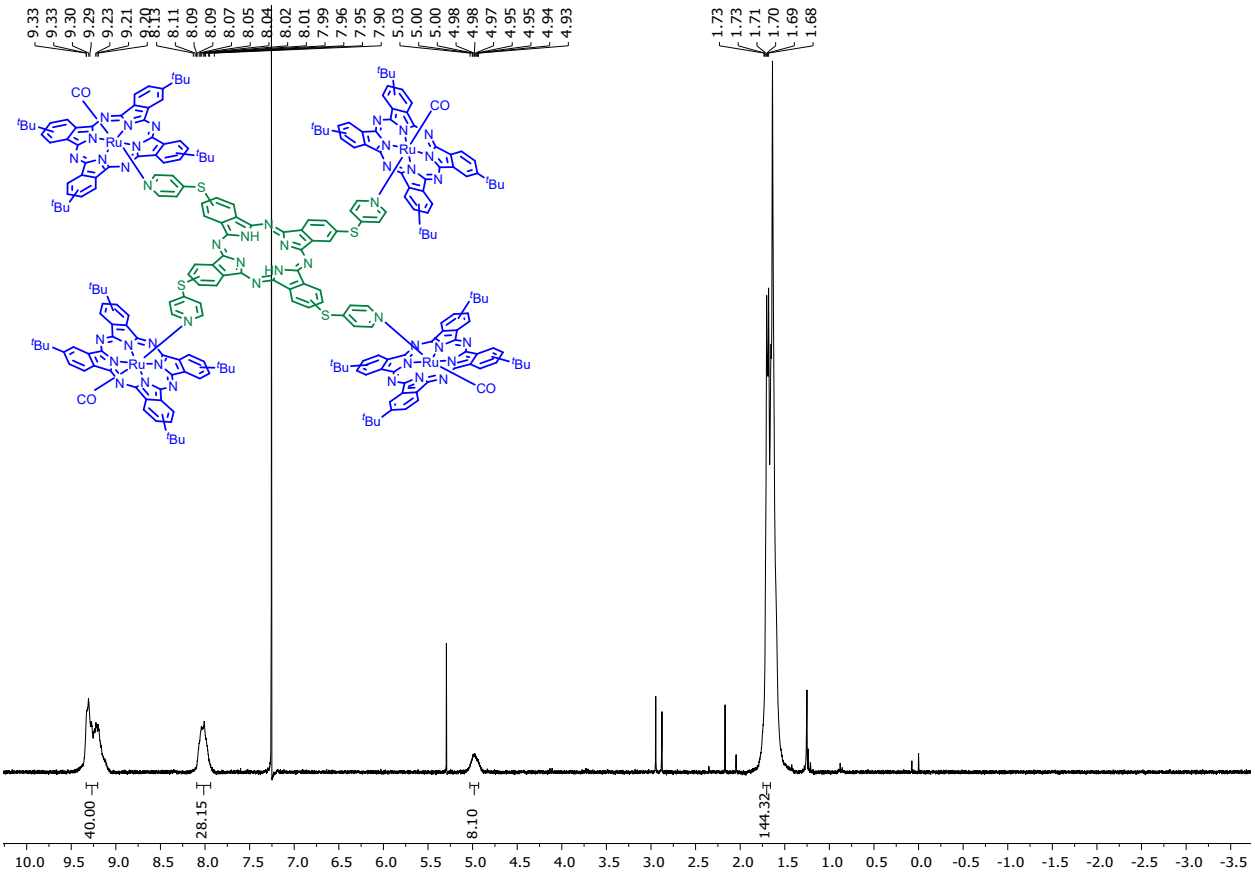

Fig. S6 ^{1}H NMR (300.13 MHz) spectrum of **3** in $CDCl_3$.

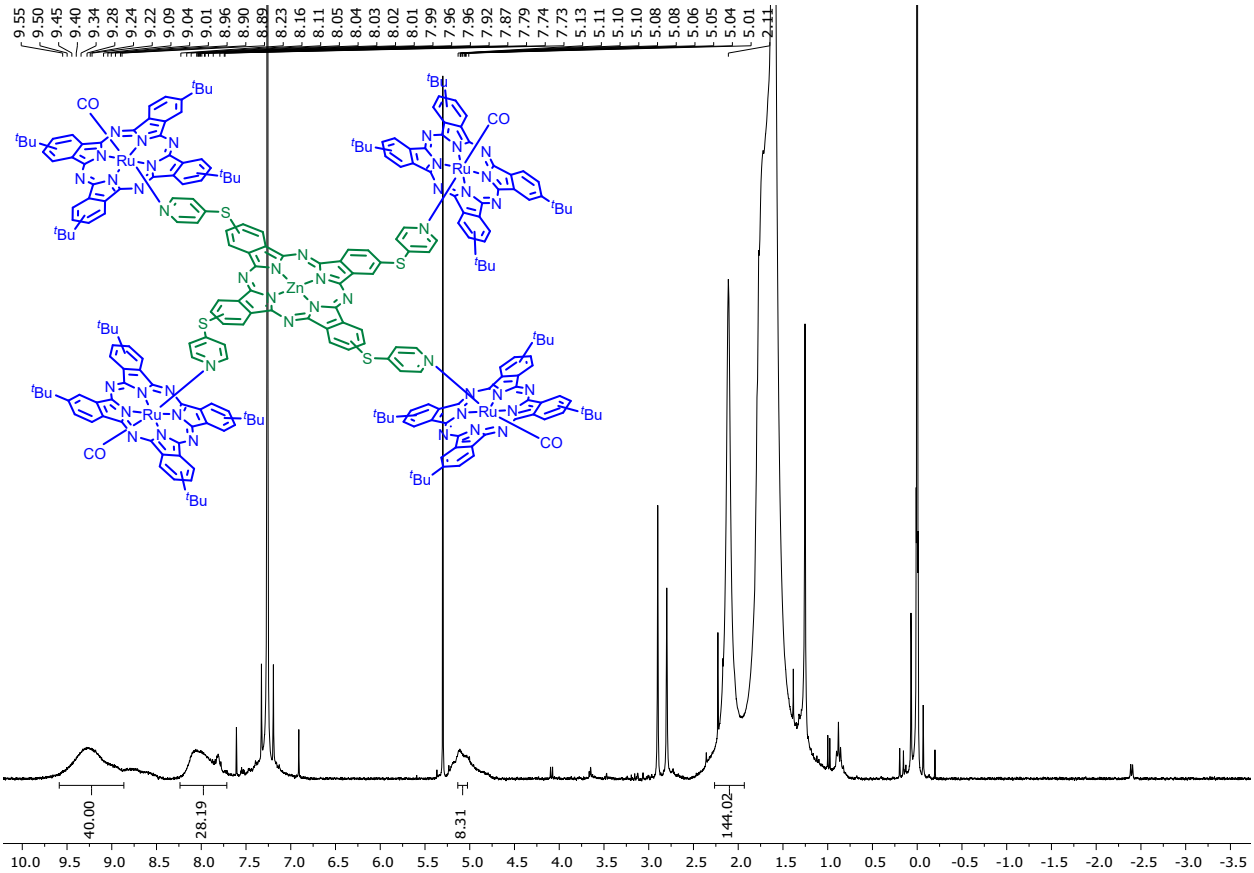

Fig. S7 ^{1}H NMR (300.13 MHz) spectrum of **4** in $CDCl_3$.

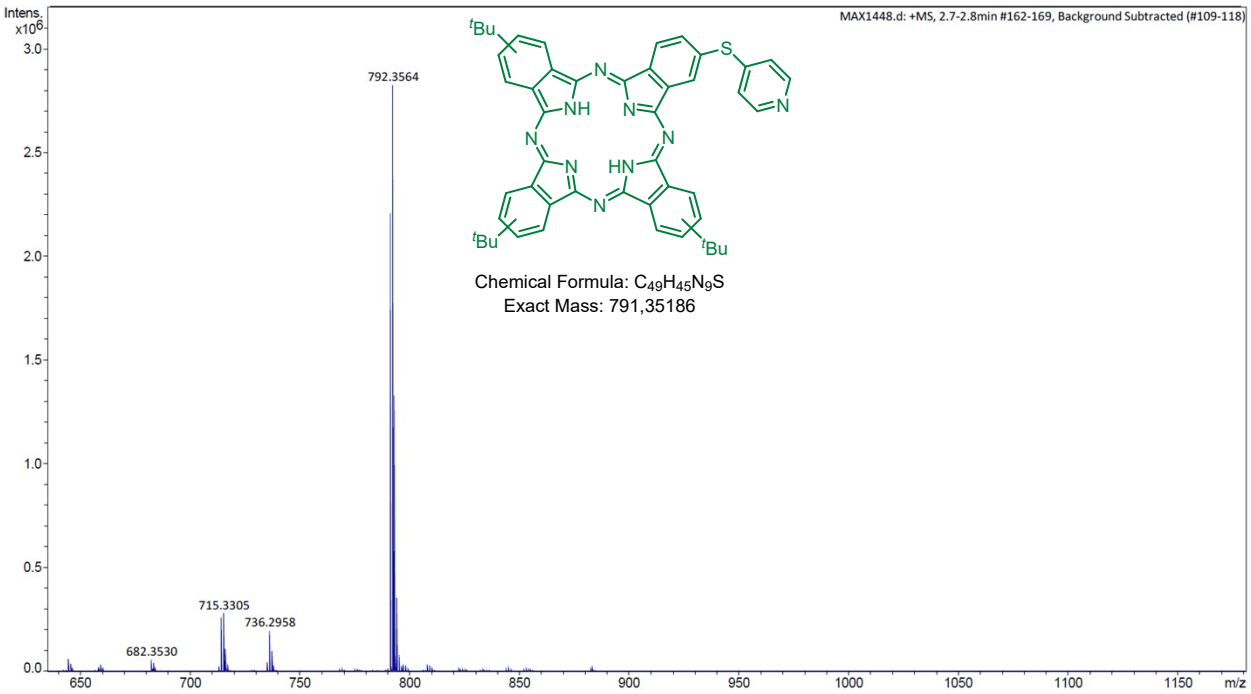

Fig. S8 HRMS spectrum of **H_2PcSPy**.

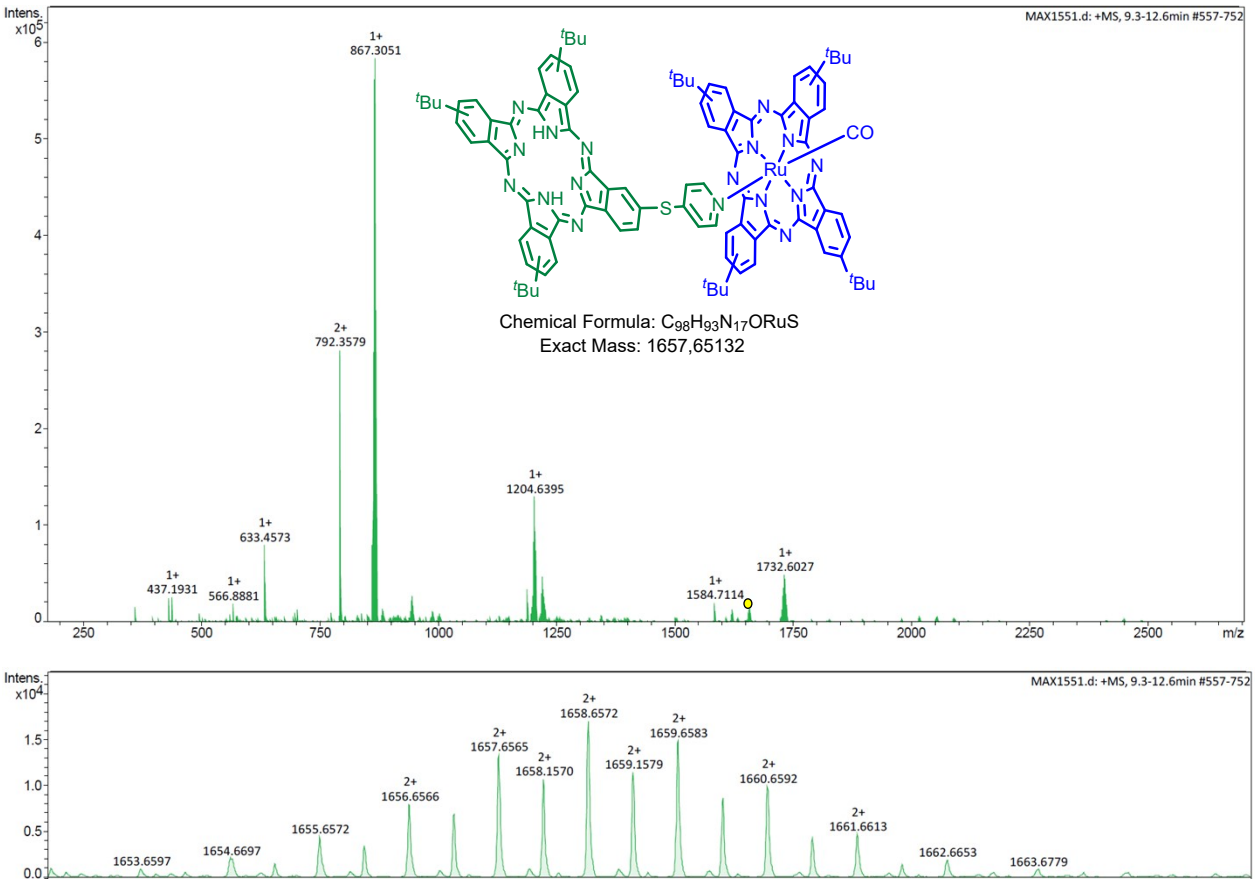

Fig. S9 HRMS spectrum of **1**. The yellow circle identifies the species of interest (*m/z* 1658.6572).

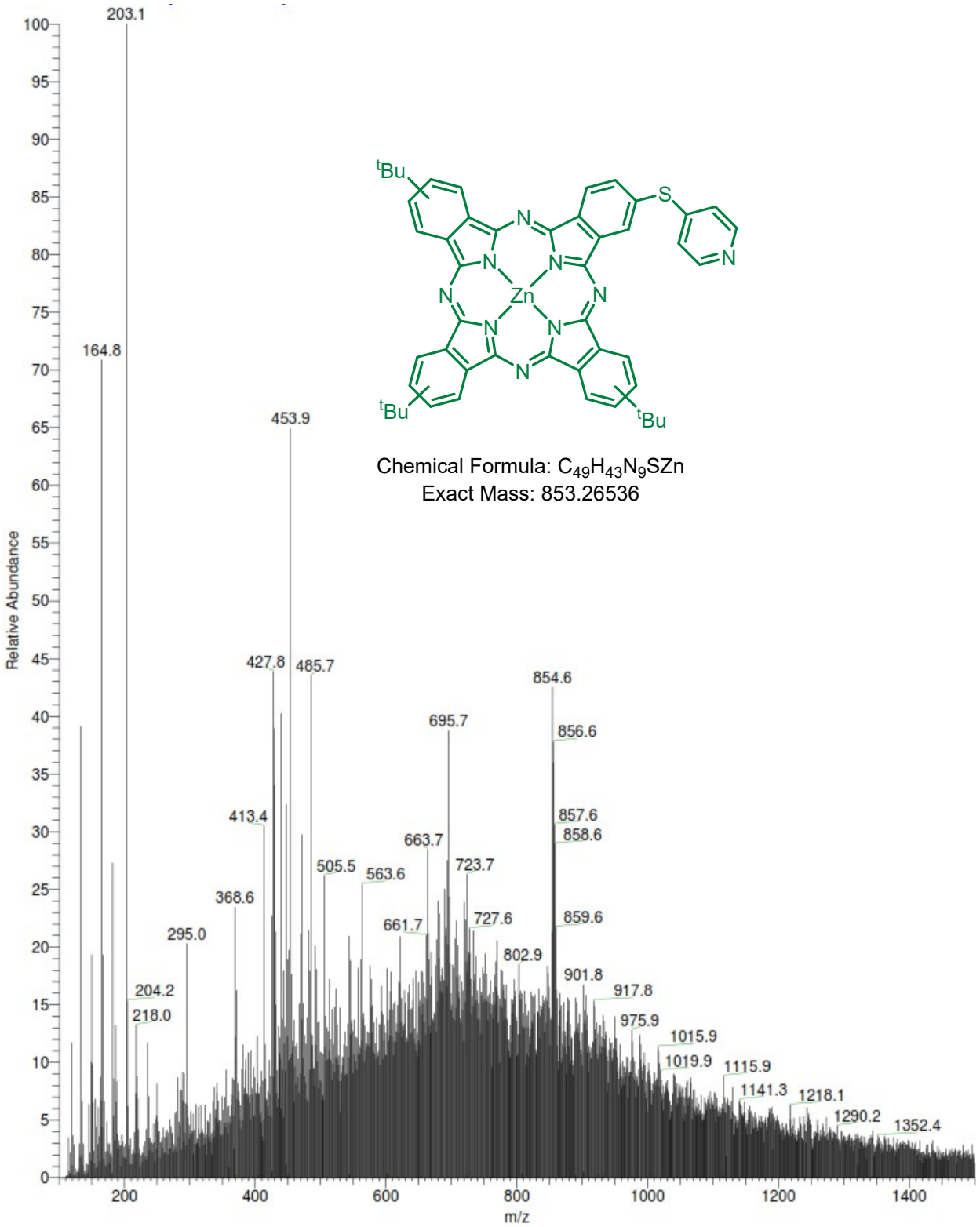

Fig. S10 MS spectrum of **ZnPcSPy**.

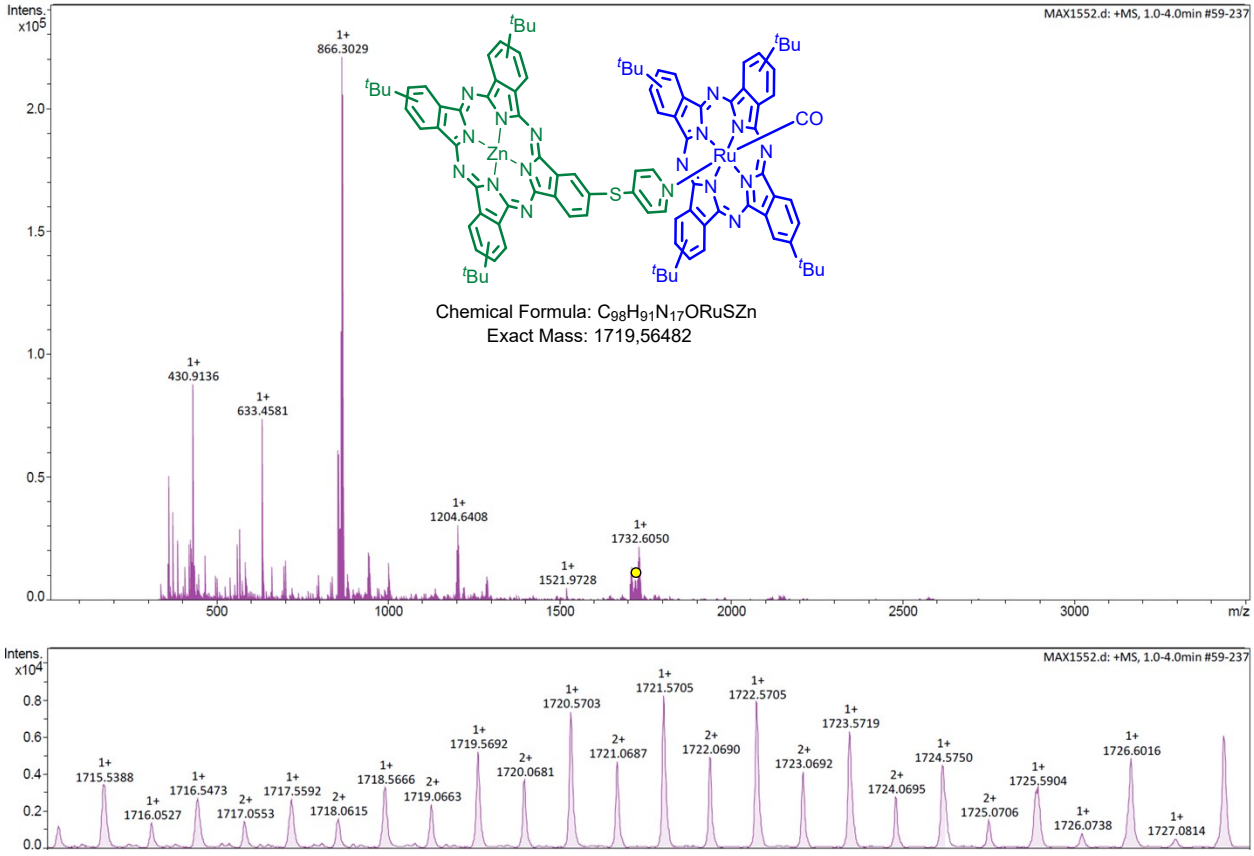

Fig. S11 HRMS spectrum of **2**. The yellow circle identifies the species of interest (*m/z* 1721.5705).

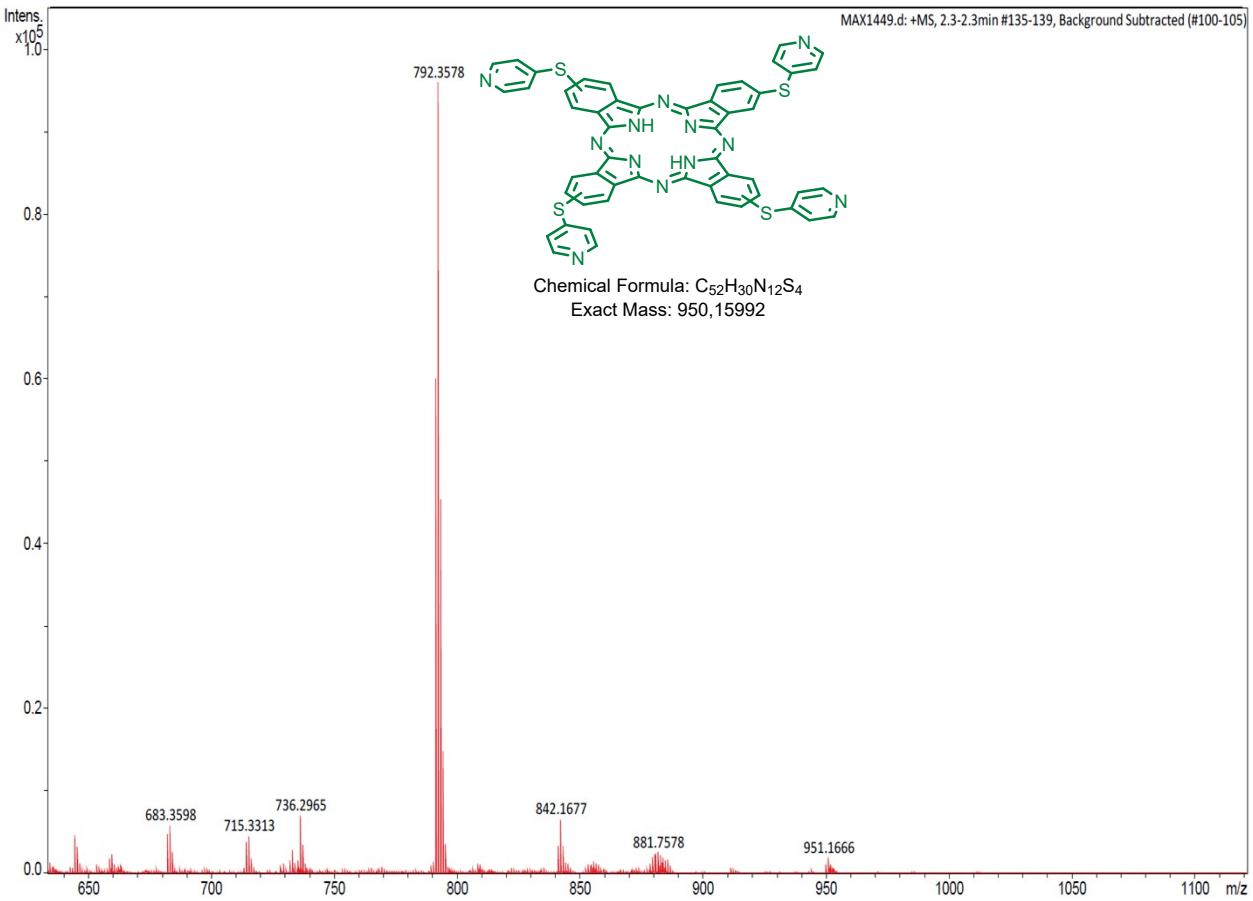

Fig. S12 HRMS spectrum of **$H_2PcH_{12}SPy_4$**.

4. Absorption spectra of all Pc dyes in CH_2Cl_2 solutions

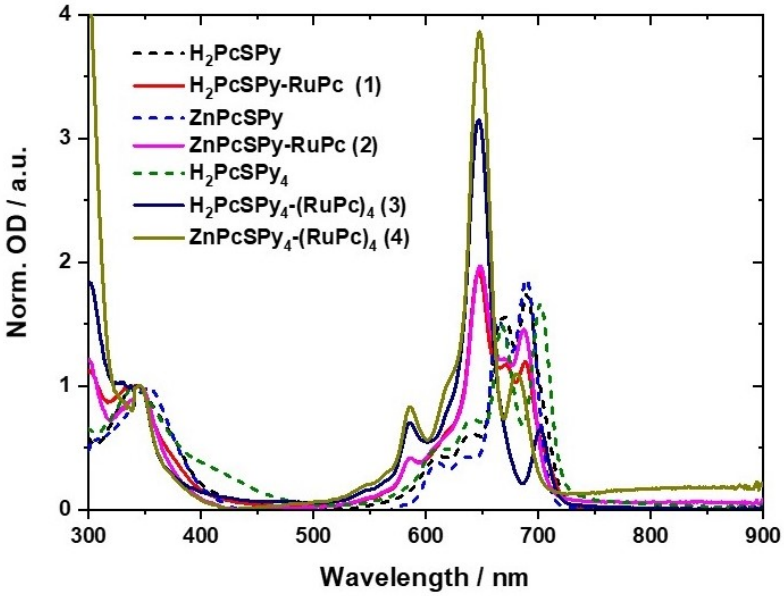

Fig. S13 Normalized absorption spectra (in the Soret band) of **H_2PcSPy**, **H_2PcSPy-RuPc 1**, **ZnPcSPy-RuPc 2**, **H_2PcSPy_4**, **H_2PcSPy_4-$(RuPc)_4$ 3**, and **$ZnPcSPy_4$-$(RuPc)_4$ 4** in CH_2Cl_2 at room-temperature.

5. Emission spectra of all Pc dyes in CH_2Cl_2 solutions

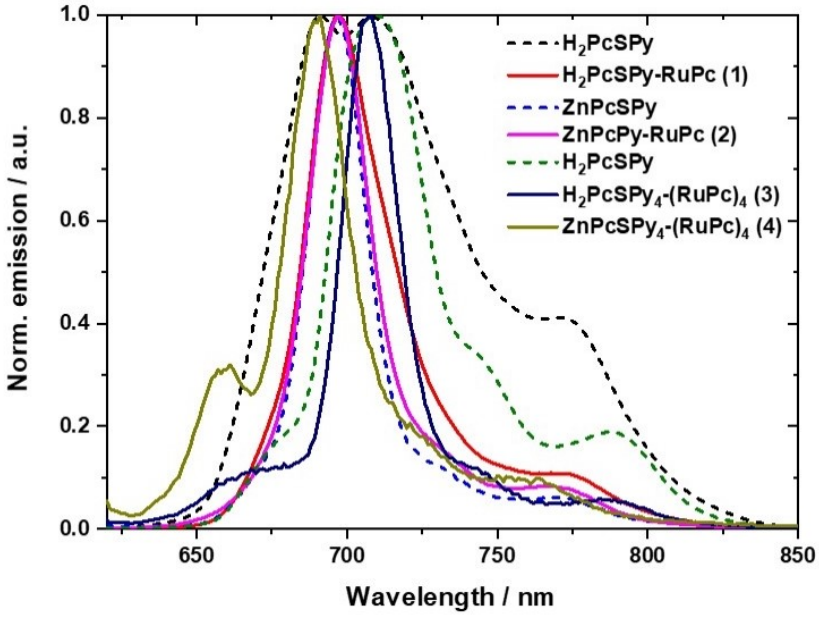

Fig. S14 Normalized emission spectra (in the Q band) of **H_2PcSPy**, **H_2PcSPy-RuPc 1**, **ZnPcSPy-RuPc 2**, **H_2PcSPy$_4$**, **H_2PcSPy$_4$-(RuPc)$_4$ 3** and **ZnPcSPy$_4$-(RuPc)$_4$ 4** in CH_2Cl_2 at room-temperature. Excitation at 610 nm.

6. Absorption spectra of Pc references in toluene solutions

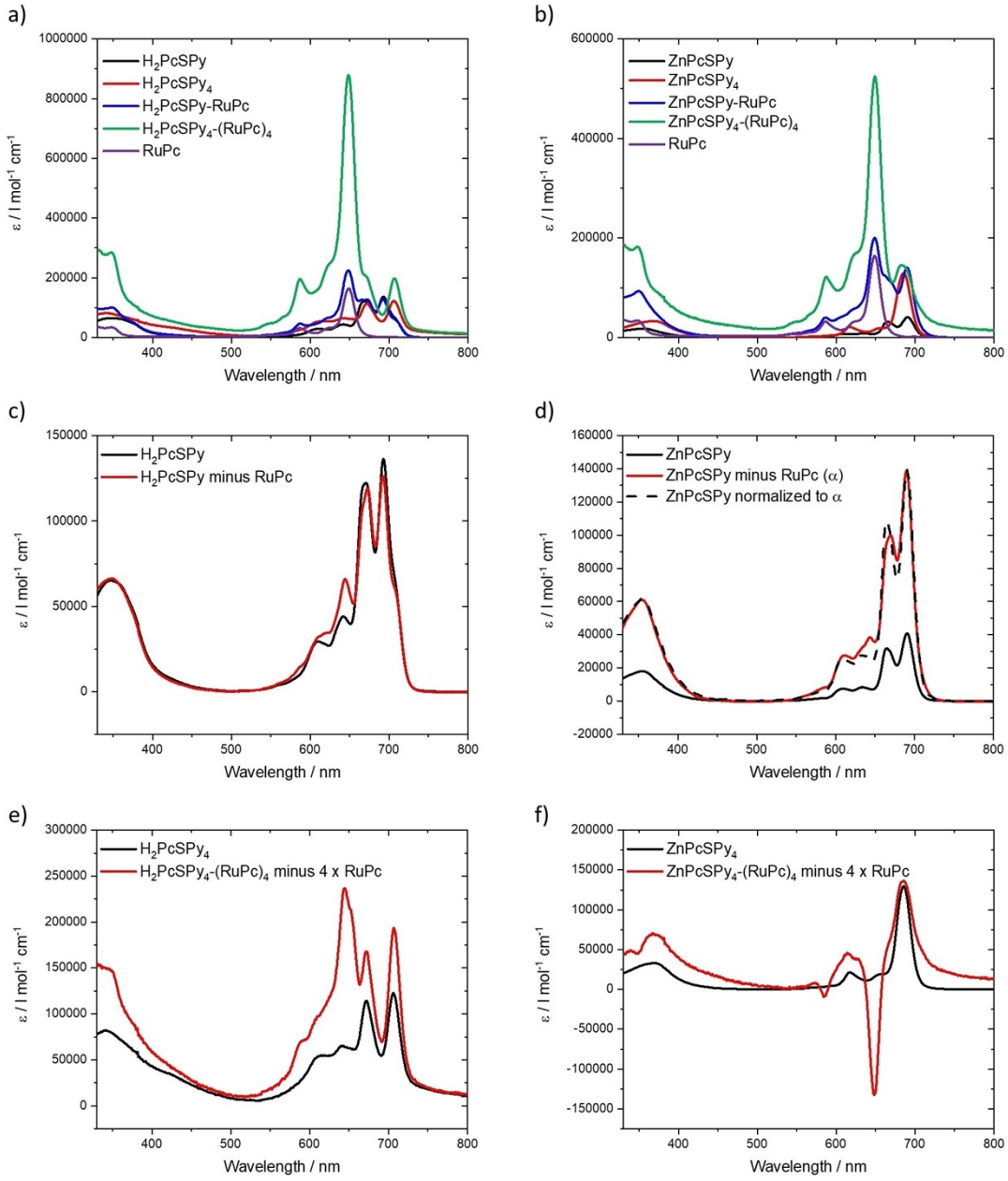

Fig. S15 Absorption spectra of a) **H_2PcSPy**, **H_2PcSPy$_4$**, **H_2PcSPy-RuPc 1**, **H_2PcSPy$_4$-(RuPc)$_4$ 3** and **RuPc**, b) **ZnPcSPy**, **ZnPcSPy$_4$**, **ZnPcSPy-RuPc 2**, **ZnPcSPy$_4$-(RuPc)$_4$ 4** and **RuPc**, c) **H_2PcSPy-RuPc** subtracted by **RuPc**, d) **ZnPcSPy-RuPc** subtracted by **RuPc**[1], e) **H_2PcSPy$_4$-(RuPc)$_4$** subtracted by 4 x **RuPc**, f) **ZnPcSPy$_4$-(RuPc)$_4$** subtracted by 4 x **RuPc** in toluene.

[1]Extinction coefficients of ZnPcSPy are more than 3× lower than expected. Considering that the normalized spectrum shows the anticipated weak ground state interactions, we assume a rather large error margin for ZnPcSPy.

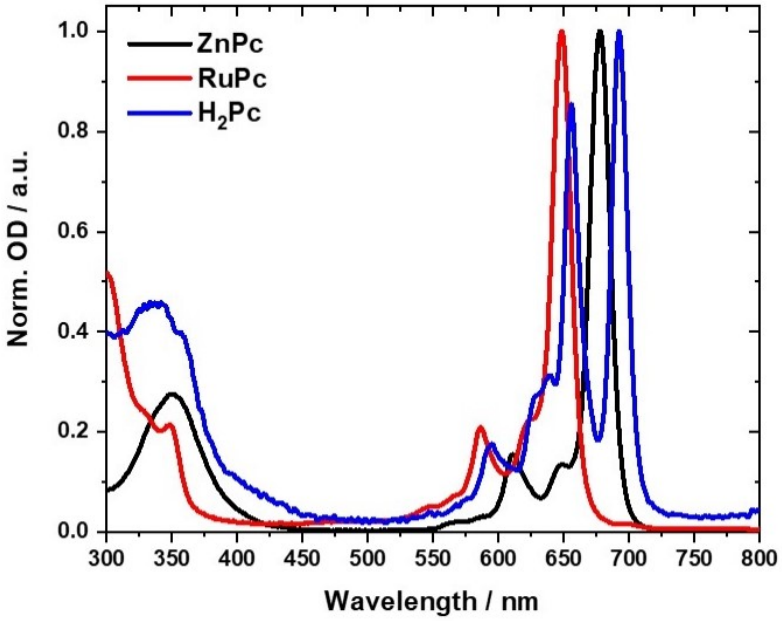

Fig. S16 Normalized absorption spectra (in the Q band) of **ZnPc**, **RuPc** and **H_2Pc** in toluene at room-temperature.

7. Emission spectra of all Pc dyes in toluene solutions

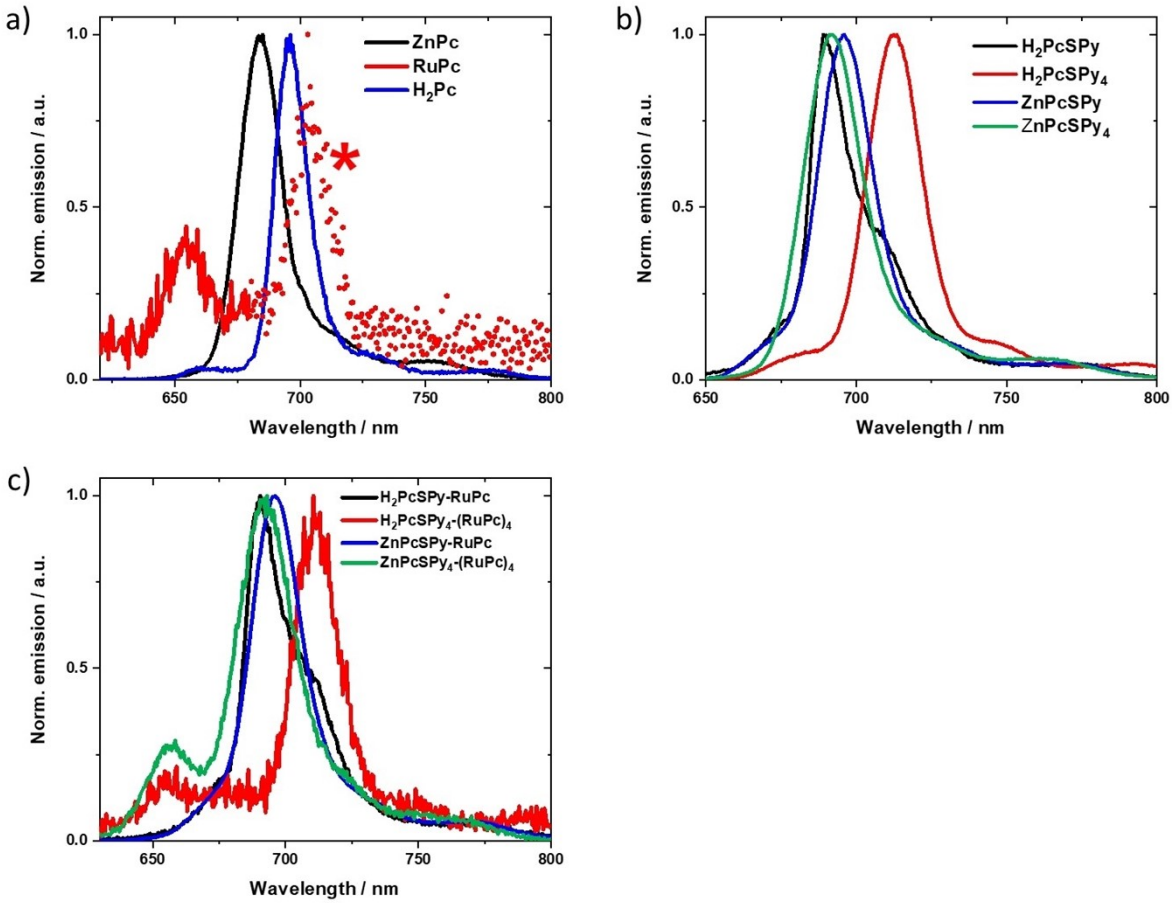

Fig. S17 Normalized emission spectra (in the Q band) of a) **ZnPc**, **RuPc**, **H_2Pc**, b) **H_2PcSPy**, **H_2PcSPy$_4$**, **ZnPcSPy**, **ZnPcSPy$_4$**, c) **H_2PcSPy-RuPc 1**, **ZnPcSPy-RuPc 2**, **H_2PcSPy$_4$-(RuPc)$_4$ 3** and **ZnPcSPy$_4$-(RuPc)$_4$ 4** in toluene at room-temperature. Excitation at 387 nm. (*minor impurities of H_2Pc).

8. Transient absorption analysis in toluene solutions

All transient absorption measurements are presented to get a quick insight into the main time resolved results obtained by applying the depicted mechanistic model in GloTarAn. Additional information such as residuals are also given to support the suggested mechanistic model and its validity.

Figure a) is a 3D map obtained by transient absorption measurements. This data was not altered in any way. The y-axis shows the time delay, at which each absorption spectrum is measured. The color code shows the intensity profile of these absorption spectra. From the bottom up, you can follow the transient absorption of different states that are involved in the decay of the excited system.

Figure b) shows the time profile of SAS obtained by GloTarAn analysis, including early signals such as IRF and coherent spectroscopic artifacts. The first and second singular vectors of the time-residual can be used to verify the results. For example, a sine curve for the first vector is a sign for an additional species that was neglected in the model.

Figure c) shows the obtained SAS spectra corresponding to the respective time profile in b). By adapting the scaling parameters of parallel pathways, all GSBs were aligned to yield the correct rate constants. The first and second singular vectors of the spectral-residual have to be examined in conjunction with the time-residuals and vice versa. If the time-residuals hint towards a species that was neglected, spectral-residuals should additionally show features that resemble the GSB or other fingerprints of SAS that are to be expected.

Figure d) depicts the applied mechanistic model. It can be considered as a simplified Jablonski scheme, for which we neglected relative energies in favor of clarity. Please note that some pathways may not be physically meaningful, such as a direct population of the CSS, but are rather an approximation of the real underlying processes due to the lack of data density at early times or ultrafast processes that are below the time resolution of our setup.

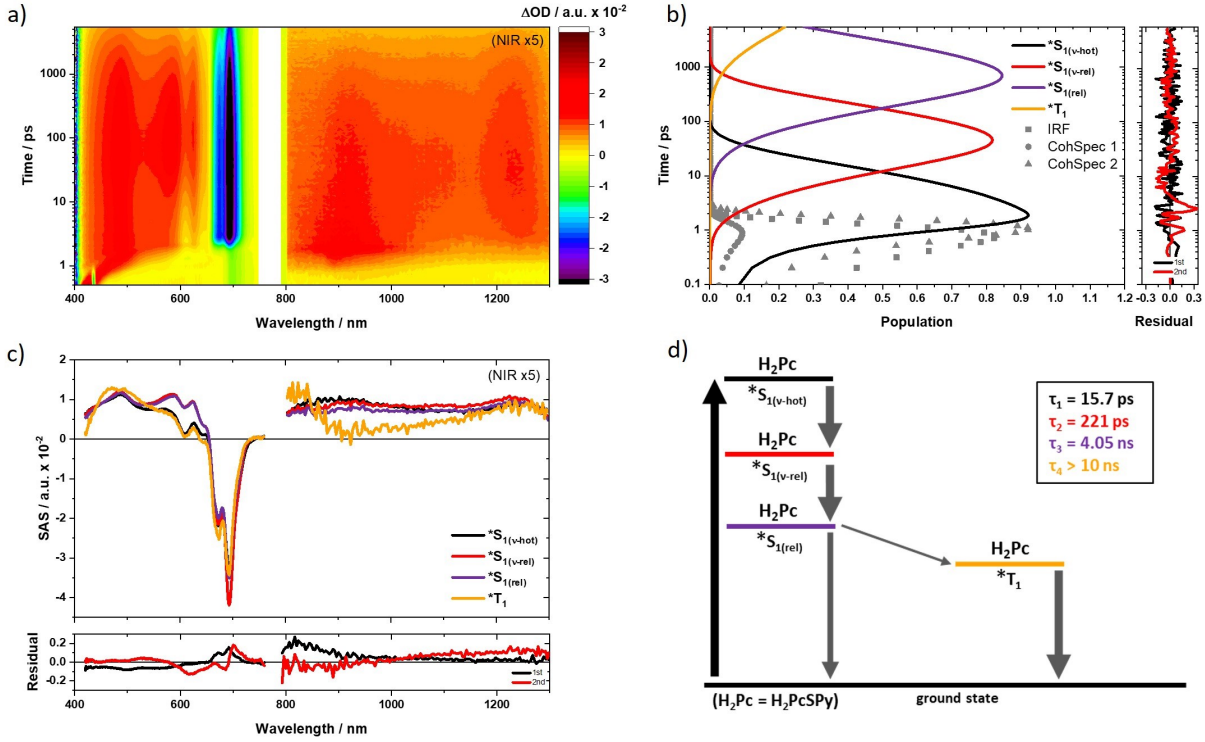

Fig. S18 a) Differential absorption spectra obtained upon femtosecond pump probe experiments (387 nm) of **H_2PcSPy** in toluene with several time delays between 0.5 and 5500 ps. b) Population over time and c) SAS obtained upon chirp corrected GloTarAn analysis of the raw data with ($^*S_{1(v\text{-}hot)}$) (black), ($^*S_{1(v\text{-}rel)}$) (red), ($^*S_{1(rel)}$) (blue), ($^*T_1$) (green), IRF (square), CohSpec 1 (circle), CohSpec 2 (triangle), and corresponding first (black) and second (red) singular vectors of the residual on the right (for b) and at the bottom (for c). d) Mechanistic model applied in GloTarAn with the arrow thickness depicting relative rate constants of excitation/deactivation events.

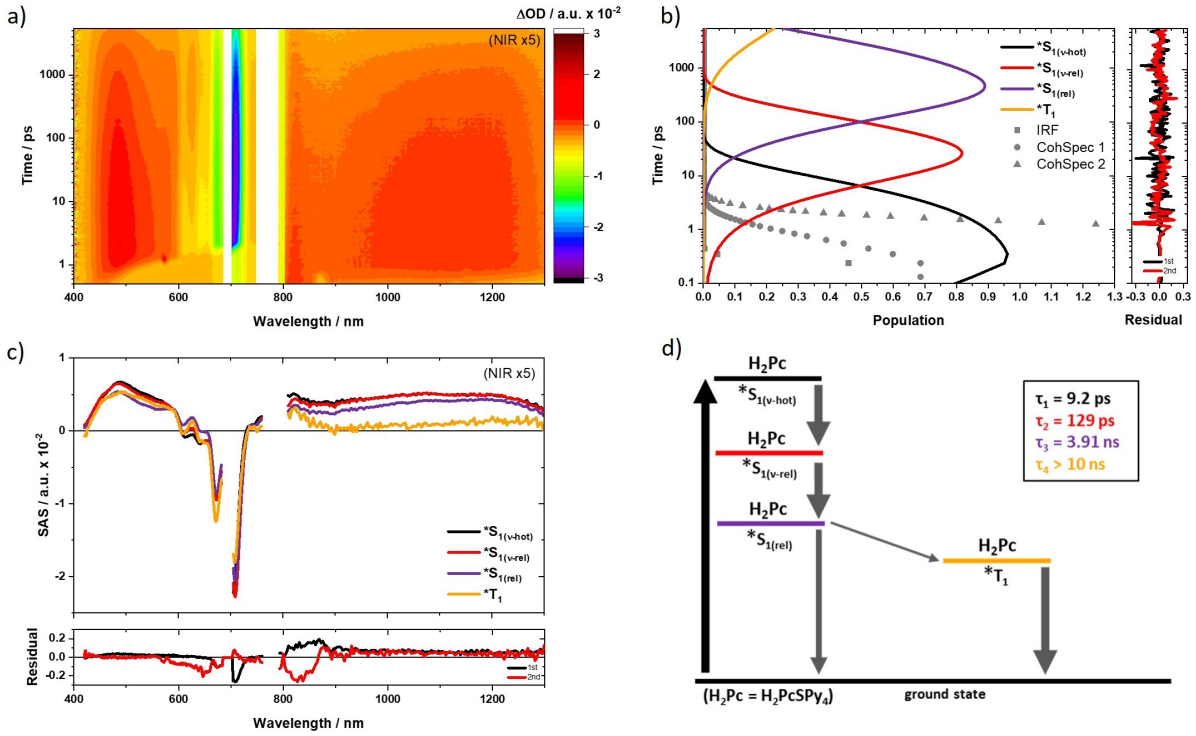

Fig. S19 a) Differential absorption spectra obtained upon femtosecond pump probe experiments (694 nm) of **H_2PcSPy$_4$** in toluene with several time delays between 0.5 and 5500 ps. b) Population over time and c) SAS obtained upon chirp corrected GloTarAn analysis of the raw data with ($^*S_{1(v\text{-hot})}$) (black), ($^*S_{1(v\text{-rel})}$) (red), ($^*S_{1(rel)}$) (blue), ($^*T_1$) (green), IRF (square), CohSpec 1 (circle), CohSpec 2 (triangle), and corresponding first (black) and second (red) singular vectors of the residual on the right (for b) and at the bottom (for c). d) Mechanistic model applied in GloTarAn with the arrow thickness depicting relative rate constants of excitation/deactivation events.

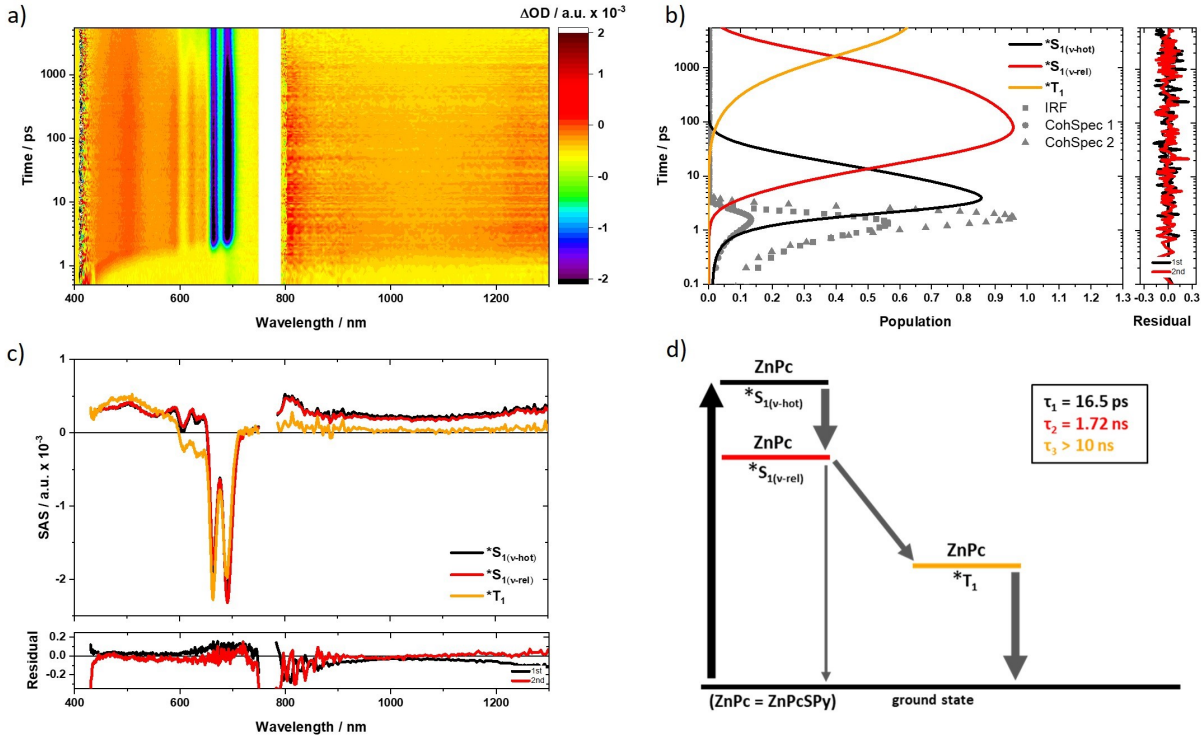

Fig. S20 a) Differential absorption spectra obtained upon femtosecond pump probe experiments (387 nm) of **ZnPcSPy** in toluene with several time delays between 0.5 and 5500 ps. b) Population over time and c) SAS obtained upon chirp corrected GloTarAn analysis of the raw data with ($^*S_{1(v\text{-}hot)}$) (black), ($^*S_{1(v\text{-}rel)}$) (red), ($^*T_1$) (blue), IRF (square), CohSpec 1 (circle), CohSpec 2 (triangle), and corresponding first (black) and second (red) singular vectors of the residual on the right (for b) and at the bottom (for c). d) Mechanistic model applied in GloTarAn with the arrow thickness depicting relative rate constants of excitation/deactivation events.

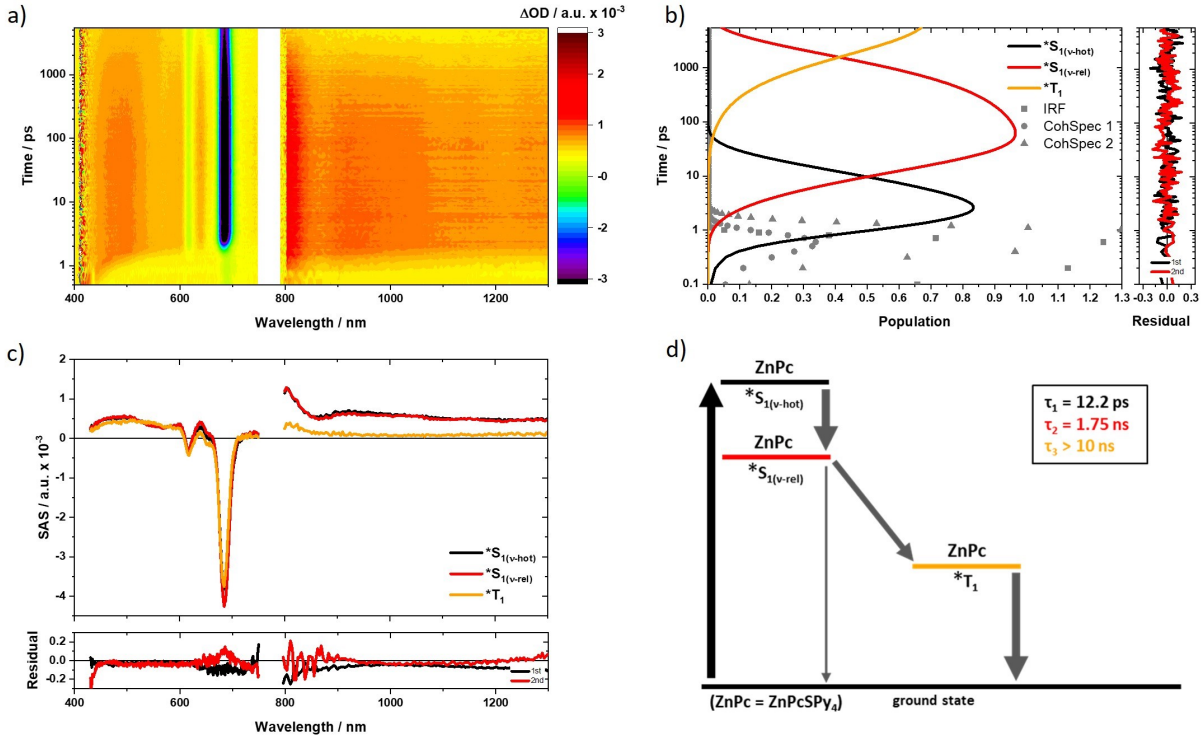

Fig. S21 a) Differential absorption spectra obtained upon femtosecond pump probe experiments (387 nm) of **ZnPcSPy$_4$** in toluene with several time delays between 0.5 and 5500 ps. b) Population over time and c) SAS obtained upon chirp corrected GloTarAn analysis of the raw data with ($^*S_{1(v\text{-}hot)}$) (black), ($^*S_{1(v\text{-}rel)}$) (red), ($^*T_1$) (blue), IRF (square), CohSpec 1 (circle), CohSpec 2 (triangle), and corresponding first (black) and second (red) singular vectors of the residual on the right (for b) and at the bottom (for c). d) Mechanistic model applied in GloTarAn with the arrow thickness depicting relative rate constants of excitation/deactivation events.

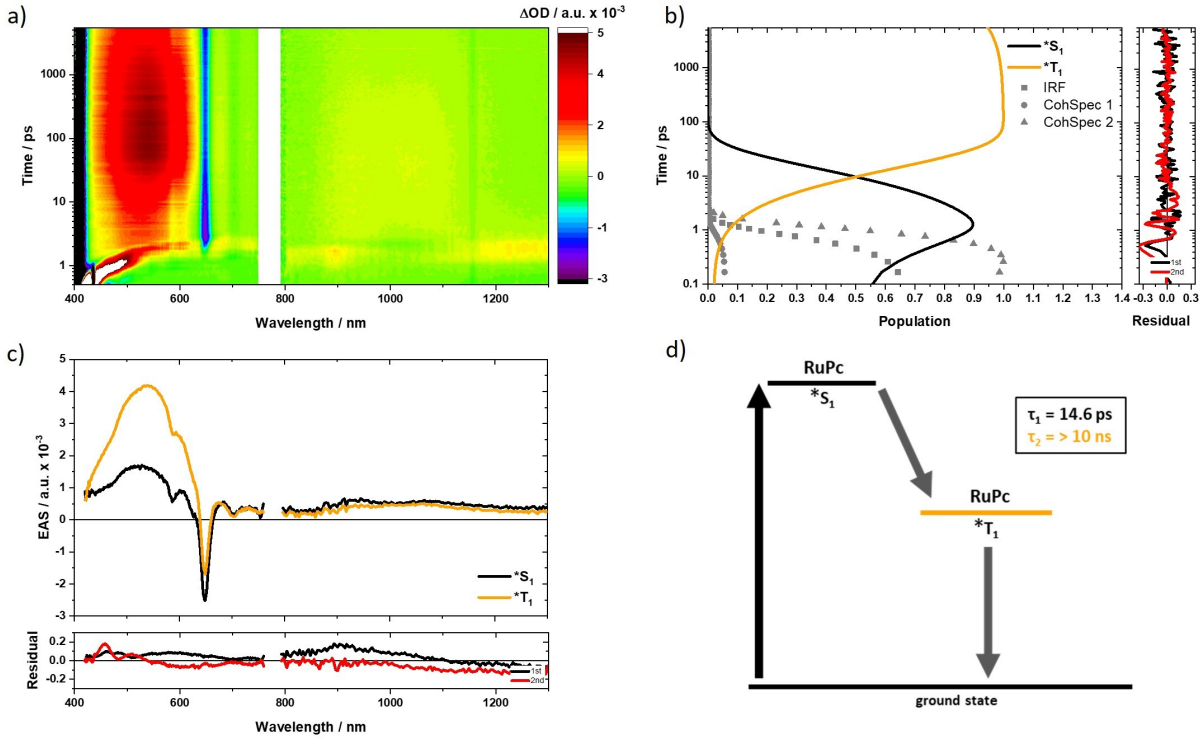

Fig. S22 a) Differential absorption spectra obtained upon femtosecond pump probe experiments (387 nm) of **RuPc** in toluene with several time delays between 0.5 and 5500 ps. b) Population over time and c) evolution associated spectra (EAS) obtained upon chirp corrected GloTarAn analysis of the raw data with ($^*S_{1(v\text{-}rel)}$) (black), ($^*T_1$) (red), IRF (square), CohSpec 1 (circle), CohSpec 2 (triangle), and corresponding first (black) and second (red) singular vectors of the residual on the right (for b) and at the bottom (for c). d) Mechanistic model applied in GloTarAn.

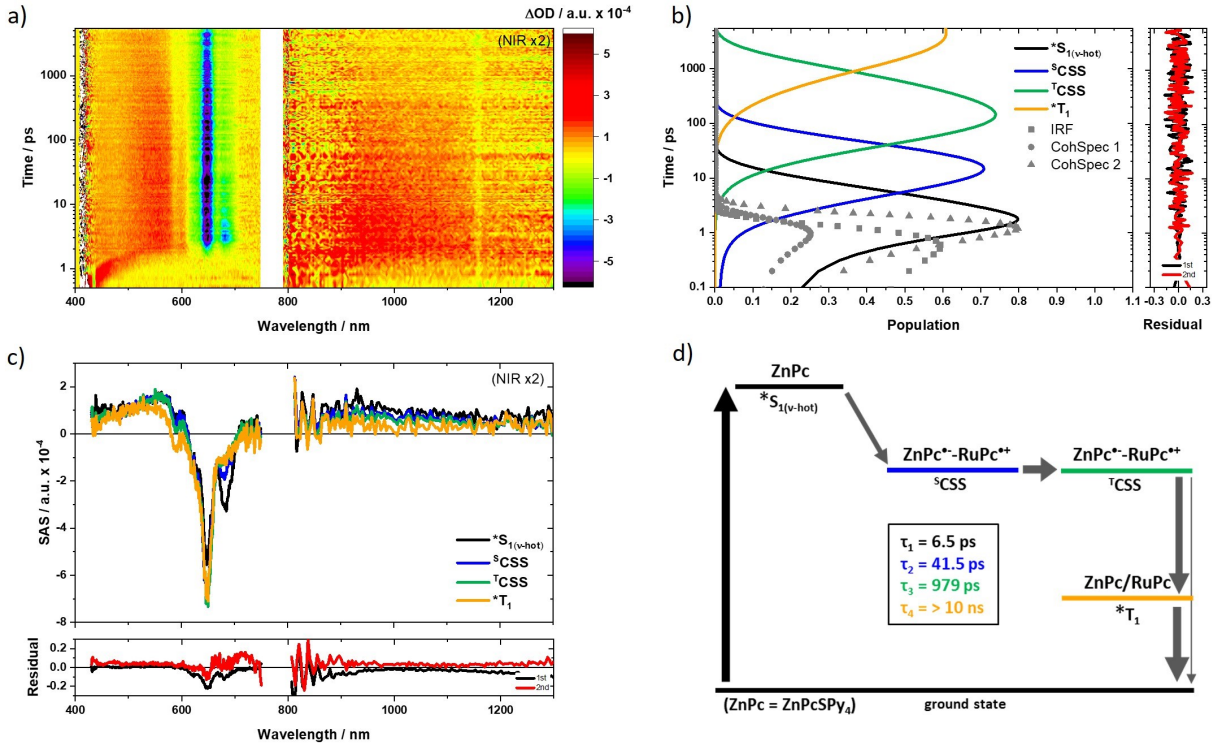

Fig. S23 a) Differential absorption spectra obtained upon femtosecond pump probe experiments (387 nm) of **4** in toluene with several time delays between 0.5 and 5500 ps. b) Population over time and c) SAS obtained upon chirp corrected GloTarAn analysis of the raw data with ($^*S_{1(v\text{-}hot)}$) (black), ^{S}CSS (red), ^{T}CSS (blue), ($^*T_1$) (green), IRF (square), CohSpec 1 (circle), CohSpec 2 (triangle), and corresponding first (black) and second (red) singular vectors of the residual on the right (for b) and at the bottom (for c). d) Mechanistic model applied in GloTarAn with the arrow thickness depicting relative rate constants of excitation/deactivation events.

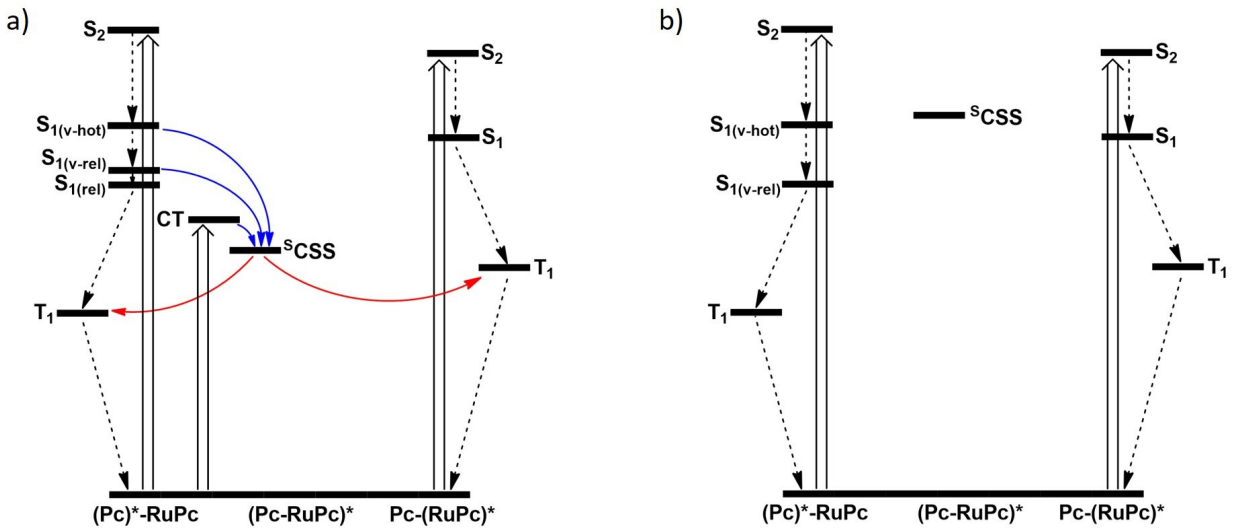

Fig. S24 Jablonski scheme of a) **1** and b) **2** derived from GloTarAn analysis of femtosecond pump-probe experiments. Charge separation and charge recombination pathways are highlighted in blue and red, respectively.